Proceedings of the Canadian Society for Mechanical Engineering International Congress
Computational Fluid Dynamics Canada International Congress
CSME - CFD-SC2023
May 28-31, 2023, Sherbrooke, QC, Canada

Modelling and Control of Dual-Motor All-Wheel Drive Electric Vehicles using Energetic Macroscopic Representation

An-Toan Nguyen[1,4*], Binh-Minh Nguyen[2], João Pedro F. Trovão[1,3], Minh C. Ta[1]

[1]Dept. of Electrical and Computer Engineering, Université de Sherbrooke, Sherbrooke, QC, J1K 2R1, Canada
[2]Dept. of Advanced Energy, the University of Tokyo, Tokyo, Japan
[3]Polytechnic of Coimbra, IPC-ISEC and INESC Coimbra, 3030-199 Coimbra, Portugal
[4]Faculty of Engineering and Technology, Quy Nhon University, Quy Nhon, Binh Dinh, Vietnam
[*]Corresponding author: An.Toan.Nguyen@USherbrooke.ca

***Abstract*—**This paper presents an Energetic Macroscopic Representation (EMR) of Electric Vehicles (EVs) with dual-motor all-wheel drive (AWD). The dynamic process of the tire-road system is considered to provide the traction force for each wheel of the studied EV. The two traction motors of the studied system including the induction motor (IM) and the permanent magnet synchronous motor (PMSM) are detailed by dynamic models. The studied EV is organized to describe the model and to design the control scheme in a more convenient way using EMR. This model is used in simulation for studying the slip phenomenon of EVs in different scenarios. The traction force is presented and analyzed for a dual-motor vehicle.

***Keywords-component*—Electric Vehicle, dual-motor all-wheel drive, longitudinal motion, dynamic model of motor, EMR**

I. Introduction

The most remarkable advantages of electric vehicles (EVs) over internal combustion engine vehicles from the motion control point-of-view reside in the use of electric motors. This can be summarized as (1) instant and accurate torque delivery for improved acceleration and responsiveness, (2) easily measurable output torque for enhanced handling and stability, and (3) regenerative braking for increased braking performance. Therefore, we should take full benefit of these advantages in the motion control design [1], [2]. To save cost and time in these studies, a dynamics model of EVs needs to be implemented to develop motion control strategies to compensate for the controllable behaviour of the vehicle.

This paper focuses on motion control of a dual-motor all-wheel drive (AWD) for EVs. The dual-motor setup of AWD-EVs provides independent control of each axle, allowing for precise control of torque distribution to each wheel. With the ability to precisely control the amount of torque going to each wheel, the AWD-EVs can operate more efficiently, using only the amount of power needed to achieve the desired performance [3], [4]. In literature, there are also some motion control studies on this configuration with various conditions on the surface road [3]- [5]. However, the number of studies on motion control and anti-slip for this configuration is still limited.

Introduced in 2000 for research in electromechanical systems, Energetic Macroscopic Representation (EMR) has been continuously developed into various energetic domains. EMR uses kinetic and potential variables based on the action-reaction principle to divide the system into comprehensively mathematical subsystems. The product of these variables on each side of a subsystem represented by EMR, is homogeneous to the power unit [6]. This approach is helpful for a complex system whose subsystems are controlled by applying the inversion-based method. Therefore, it has the great advantage of its clearness and simplicity of control design. However, the existing EMR with a focus on energy studies merely simplifies the vehicle dynamics without considering the dynamic process of the tire-road system. Furthermore, to acquire high-performance motion characteristics, the traction force of the motor should be regulated to maintain good traction behavior. Therefore, a dynamic model of EVs using EMR that considers the effect of the tire-road friction coefficient is needed to complete studied about energy and motion control.

In this paper, the AWD-EVs model considering the tire-road interaction is described by EMR. Here, dual-motor is also represented by a dynamic model in EMR. They are presented in Section II. Next, the maximal control organization and the estimation using the inversion-based method by EMR is depicted in Section III. Section IV provides the simulation results. The conclusion and future work are given in Section V.

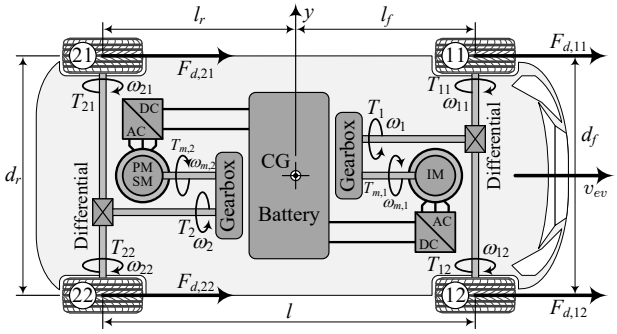

Figure. 1. Modeling of studied vehicle dynamics.

II. Configuration and Modelling

A. Configuration of the studied vehicle

The model of the studied EV is presented in Fig. 1, in which the kinematic variables of this EV model are denoted as follows: v_{ev} is the vehicle velocity at the center of gravity (CG); d_f and d_r are front and rear wheel-tracks, respectively; l_f and l_r are the distances between the vehicle CG and the front and rear axles, respectively; and l is the vehicle wheelbase.

The studied vehicle uses two different electric motors (EMs), the induction motor (IM) and the permanent magnet synchronous motor (PMSM), in the front and rear axles of this vehicle, respectively. In order to minimize the number of equations presented, the later part of this paper will present variables and equations commonly to similar elements of the front and rear axles, where the subscript "i" stands for "1" and "2" as a function of the elements of the front and rear axles, respectively. In addition, this paper also uses the subscript "j" to denote "1" and "2" corresponding to the variables of the left and right wheels of each axle, respectively. The dynamic variables are denoted as follows: torque developed by motors $T_{m,i}$, angular speed of motors $\omega_{m,i}$, torque of wheels T_{ij}, angular speed of wheels ω_{ij}, traction forces on the wheel $F_{d,ij}$.

B. Modelling of the Studied EV System

The EV model using EMR is given in Fig. 2. All the mathematical equations for modeling are provided in Table I.

1) Battery: The battery cell electrical model u_{cell} can be modeled by (1). The cell open-circuit voltage $u_{cell,OC}$ is a non-linear function of the state-of-charge (SoC) and r_{cell} is the equivalent series resistance. The Coulomb counting is used to calculate the SoC of each cell SoC_{cell}. Because the cells are connected in series and parallel, the relationships of the voltage and current of the battery and a cell can be given by (2); in which n_s is the number of cells connected in series and n_p is the number of parallel branches. The battery pack is depicted by EMR source element green oval pictogram that outputs the voltage u_{bat} and inputs the current i_{bat} in Fig. 2.

2) Parallel Connection: The parallel connection being used to supply two EMs with only one battery pack, the voltage supplied to the inverters of EMs is u_{bat} (3). The battery current i_{bat} is equal to sum of the inverter currents $i_{inv,i}$ and are given by (3). These currents $i_{inv,i}$ are split depending on the demand of each EM. In Fig. 2, this parallel connection is described by a coupling element stacked orange squares pictogram in EMR.

TABLE. I
Equations for Modelling of the Studied EV System

Modelling of the Studied EV System

$$\begin{cases} u_{cell} = u_{cell,OC}(SoC) - r_{cell} i_{cell} \\ SoC_{cell} = SoC_{cell}(0) - \dfrac{1}{C_{eq}} \displaystyle\int_0^t i_{cell} \mathrm{d}t \end{cases} \quad (1)$$

$$\begin{cases} u_{bat} = u_{cell} n_s \\ i_{cell} = \dfrac{i_{bat}}{n_p} \end{cases} \quad (2) \qquad \begin{cases} u_{bat} \text{ common} \\ i_{bat} = \displaystyle\sum_{i=1}^{2} i_{inv,i} \end{cases} \quad (3)$$

$$\begin{cases} T_i = k_{gb,i} T_{m,i} \eta_{gb,i}^{k_{tr,i}} \\ \omega_{m,i} = k_{gb,i} \omega_i \end{cases}, \text{ with } k_{tr,i} = \begin{cases} 1 & \text{if } T_i \omega_i \geq 0 \\ -1 & \text{if } T_i \omega_i < 0 \end{cases} \quad (4)$$

$$\begin{cases} T_{ij} = k_{dif,ij} T_i \eta_{dif,i}^{k_{tr,i}} \\ \omega_i = k_{dif,ij} \omega_{ij} \end{cases} \quad (5) \qquad \omega_{ij} = \frac{1}{\widetilde{J}_{\omega,ij}} \int_0^t \left(T_{ij} - T_{d,ij}\right) \mathrm{d}t \quad (6)$$

$$F_{d,ij} = \mu_{ij} F_{z,ij} \sin\left\{ C \arctan\left[B\lambda_{ij} - E\left(B\lambda_{ij} - \arctan(B\lambda_{ij})\right)\right]\right\} \quad (7)$$

$$F_{z,ij} = mg\frac{l_i}{2l} + ma\frac{k_x h_{CG}}{2l} \quad (8)$$

$$\lambda_{ij} = \frac{\Delta v_{ij}}{\max\left(R_{wh,ij}\omega_{ij}, v_{ev}, \varepsilon\right)} \quad (9) \qquad \begin{cases} \Delta v_{ij} = R_{wh,ij}\omega_{ij} - v_{ev} \\ T_{d,ij} = R_{wh,ij} F_{d,ij} \end{cases} \quad (10)$$

$$\begin{cases} F_{d,tot} = \displaystyle\sum_{i=1}^{2}\sum_{j=1}^{2} F_{d,ij} \\ v_{ij} = v_{ev} \end{cases} \quad (11) \qquad v_{ev} = \frac{1}{m}\int_0^t \left(F_{d,tot} - F_{res}\right)\mathrm{d}t \quad (12)$$

$$F_{res} = k_{roll} mg\cos\alpha + 0.5\rho c_d A_x (v_{ev} + v_{wind})^2 + mg\sin\alpha \quad (13)$$

3) Inverter and EM: The inverter and EM form an electrical drive system that converts electrical energy into mechanical energy. Thus each electrical drive is represented by a multi-physical conversion element orange circle pictogram in EMR (Fig. 2), and will be modelled in detail in Fig. 3. These two motors in the studied EV described by the mathematical equations in Table II. In these traction motor models, some variables will be bold to indicate that they are the vectors or the matrices.

The two voltage source inverters are used to convert a DC input voltage into their AC to supply two motors. The inverters output voltage $\boldsymbol{u}_{inv,i}$ and the DC input current i_{inv} as shown in (14) are proportional to the DC voltage of the battery u_{bat} and the AC currents of the motor $\boldsymbol{i}_{em,i}$, respectively; in which $\boldsymbol{m}_{inv,i}$ is the amplitude modulation of each inverter, and $\eta_{dr,i}$ is the efficiency of the drive system including the inverter and the electric motor. Each voltage source inverter is represented by mono-physical conversion element orange square pictogram in EMR (Fig. 3).

For motor model analysis, the stationary a-b-c frame is converted to the rotating d-q frame and vice versa using Park transformation. Hence, the voltage and current transforms can be given by (15)-(16); where $u_{d,i}$, $u_{q,i}$, $i_{d,i}$, $i_{q,i}$ symbolize the voltages and currents in the d-q frame transformed from a-b-c frame according to the rotor position θ_i; $\boldsymbol{T}_{PC}$, $\boldsymbol{T}_{CP}$, $\boldsymbol{T}_v$, and $\boldsymbol{T}_c$ are the frame transformation matrices [7]. This

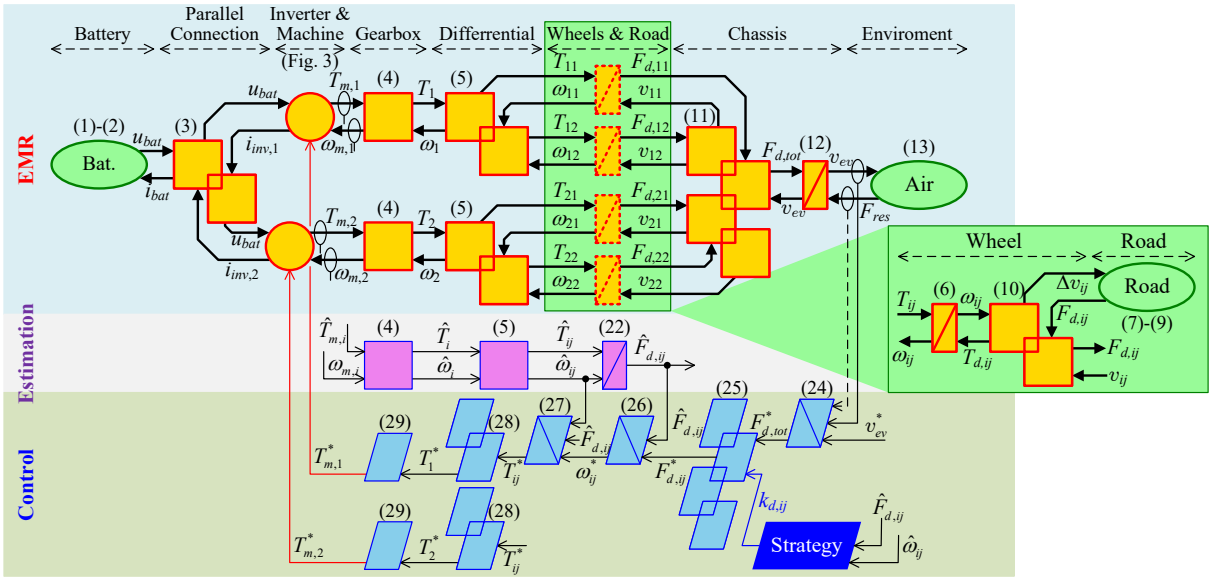

Figure. 2. EMR and control scheme of studied vehicle.

TABLE. II
EQUATIONS FOR MODELLING OF THE STUDIED EMS

Modelling of the Studied EMs

$$\begin{cases} \boldsymbol{u}_{inv,i} = \begin{bmatrix} u_{ac,i} \\ u_{bc,i} \end{bmatrix} = \boldsymbol{m}_{inv,i} u_{bat} \\ i_{inv,i} = \boldsymbol{m}_{inv,i}^T \begin{bmatrix} i_{a,i} \\ i_{b,i} \end{bmatrix} \eta_{dr,i}^{k_{inv}} = \boldsymbol{m}_{inv,i}^T \boldsymbol{i}_{em,i} \eta_{dr,i}^{k_{inv,i}} \\ \boldsymbol{m}_{inv,i} = \begin{bmatrix} m_{ac,i} \\ m_{bc,i} \end{bmatrix} \end{cases} \tag{14}$$

$$\text{with } k_{inv,i} = \begin{cases} -1 & \text{if } u_{bat,i} i_{inv,i} \geq 0 \\ 1 & \text{if } u_{bat,i} i_{inv,i} < 0 \end{cases}$$

$$\boldsymbol{u}_{dq,i} = \begin{bmatrix} u_{sd,i} \\ u_{sq,i} \end{bmatrix} = \boldsymbol{T}_{PC} \boldsymbol{T}_v \boldsymbol{u}_{inv,i} \tag{15}$$

$$\boldsymbol{i}_{em,i} = \begin{bmatrix} i_{a,i} \\ i_{b,i} \end{bmatrix} = \boldsymbol{T}_c \boldsymbol{T}_{CP} \begin{bmatrix} i_{sd,i} \\ i_{sq,i} \end{bmatrix} = \boldsymbol{T}_c \boldsymbol{T}_{CP} \boldsymbol{i}_{dq,i} \tag{16}$$

$$\boldsymbol{i}_{dq,i} = \begin{bmatrix} i_{sd,i} \\ i_{sq,i} \end{bmatrix} = \begin{bmatrix} \dfrac{1}{R_{s,i} + \mathrm{s}L_{sd,i}} (u_{sd,i} - e_{sd,i}) \\ \dfrac{1}{R_{s,i} + \mathrm{s}L_{sq,i}} (u_{sq,i} - e_{sq,i}) \end{bmatrix} \tag{17}$$

$$\boldsymbol{e}_{dq,i} = \begin{bmatrix} e_{sd,i} \\ e_{sq,i} \end{bmatrix} = \begin{bmatrix} -\omega_{s,i} L_{sq,i} i_{sq,i} \\ \omega_{s,i} L_{sd,i} i_{sd,i} + e_{\lambda,i} \end{bmatrix} \tag{18}$$

$$\text{with} \begin{cases} \omega_{s,i} = \begin{cases} p_{p,1}\omega_{m,1} + \dfrac{R_{r,1}}{L_{r,1}} \cdot \dfrac{L_{m,1}}{\lambda_{rd,1}} i_{sq,1} & \text{if IM} \\ p_{p,2}\omega_{m,2} & \text{if PMSM} \end{cases} \\ e_{\lambda,i} = \begin{cases} \omega_{s,1} \dfrac{L_{m,1}}{L_{r,1}} \lambda_{rd,1} & \text{if IM} \\ \omega_{s2} \Phi_{r,2} & \text{if PMSM} \end{cases} \end{cases}$$

$$\lambda_{rd,1} = \frac{R_{r,1} L_{m,1}}{R_{r,1} + \mathrm{s}L_{r,1}} i_{sd,1} \tag{19}$$

$$\theta_i = \int_0^t \omega_{s,i} \mathrm{d}t \tag{20}$$

$$\begin{cases} T_{m,1} = \dfrac{3}{2} p_{p,i} \dfrac{L_{m,1}}{L_{r,1}} \lambda_{rd,1} i_{sq,1} \\ T_{m,2} = \dfrac{3}{2} p_{p,2} \left[\Phi_{r,2} i_{sq,2} + (L_{sd,2} - L_{sq,2}) i_{sd,2} i_{sq,2} \right] \end{cases} \tag{21}$$

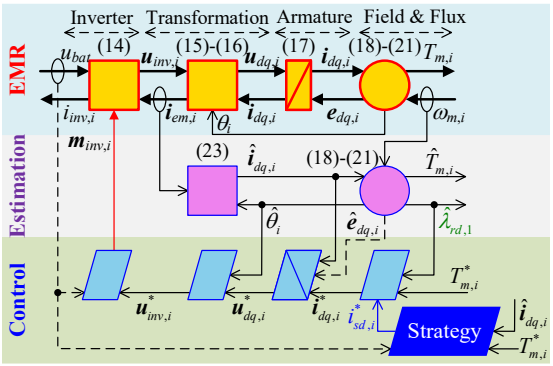

Figure. 3. EMR and control scheme of studied motors.

is represented as a mono-physical conversion element orange square pictogram in Fig. 3.

Based on the mathematical modelling of IM and PMSM in d-q frame, the relation between current, voltage and back-electromotive-force (EMF) of each motor is described as (17); in which $R_{s,i}$, $L_{sd,i}$, and $L_{sq,i}$ are define as the resistance, d-axis inductance and q-axis inductance of the stator (armature winding), respectively. For IM, $L_{sd,1} = L_{sq,1} = \sigma L_{s,1}$, $\sigma = 1 - L_{m,1}^2/(L_{s,1}L_{r,1})$; with $L_{s,1}$, $L_{r,1}$ and $L_{m,1}$ are the stator, rotor and magnetisation inductance of IM. The EMF in the stator is expressed in (18)-(19); in which $\omega_{s,i}$ is the synchronous speed, $p_{p,i}$ is the number of pole pair, $R_{r,1}$ is the rotor resistance of IM, $\lambda_{rd,1}$ is the rotor flux of IM, $\Phi_{r,2}$ is the rotor flux from permanent magnets of PMSM. The armature element of the motors is depicted as an accumulation element orange rectangle pictogram with diagonal in EMR (Fig. 3).

The rotor position θ_i is modeled by (20). The motor torque $T_{m,i}$ is then generated by the interaction between the induced flux in the rotor of IM (or the permanent magnet in the rotor

of PMSM) and the stator current, which can be represented as (21). This dynamic equation is described by a multi-physical conversion element orange circle pictogram in Fig. 3.

4) Gearbox: The gearbox converts the mechanical power coming from the EM to the differential (mono-physical conversion element orange square pictogram in EMR). These gearbox blocks are expressed by (4), which is dependent on the ratio of the gearbox $k_{gb,i}$, the gearbox efficiency $\eta_{gb,i}$ (assumed to be constant), the angular speed of the differential ω_i, and the power flow direction indicator $k_{tr,i}$.

5) Differential: The differential distributes the mechanical power coming from the gearbox to the wheel (coupling element stacked orange squares pictogram in EMR). These differential blocks are modelled by (5), which is dependent on the distribution ratio of the differential $k_{dif,ij}$ (assumed here to be 0.5), the differential efficiency $\eta_{dif,i}$ (assumed to be constant), the angular speed of the wheel ω_{ij}, and the power flow direction indicator $k_{tr,i}$.

6) Wheel: The torque and angular speed from each differential are converted to the torque and angular speed of each respective wheel. The angular speed of each wheel ω_{ij} is computed using the equivalent dynamic equation for each wheel (6); in which $\widetilde{J}_{\omega,ij} = J_{wh,ij} + J_{m,i}k_{gb,i}^2 k_{dif,ij}^2$ is the equivalent rotational inertia moment of each wheel plus the equivalent rotational inertia moment of each EM and $T_{d,ij}$ is the torque of each wheel depending on the longitudinal force of each wheel $F_{d,ij}$. This dynamic equation is described by an accumulation element orange rectangle pictogram with diagonal in EMR (Fig. 2).

The "magic formula" proposed by Pacejka in [8] is used to generally describe longitudinal forces, as (7); in which μ_{ij} is the friction coefficient, and B, C and E are the shape factors in the "magic formula" tire model. The vertical force $F_{z,ij}$ which is the load transfer caused by longitudinal acceleration are calculated as (8); in which m is total mass considered as the sum of the studied EV net weight and the driver, g is the gravity acceleration, a denote the longitudinal acceleration of the vehicle, h_{CG} is the height of CG, $k_x = -1$ if $i = 1$, $k_x = 1$ if $i = 2$, $l_i = l_r$ if $i = 1$, $l_i = l_f$ if $i = 2$.

The slip ratio λ_{ij} is defined as (9) which is produced by a difference between the tire rolling velocity and its travel velocity. In (9), Δv_{ij} is the difference between vehicle velocity v_{ev} and wheel velocity (10), $R_{wh,ij}$ is the radius of the wheel (ε is a small positive value to avoid division by zero).

A source element green oval pictogram in EMR (Road) is used to describe the interaction between the wheel (tire) and the road surface in Fig. 2. This element output is the longitudinal force $F_{d,ij}$, and the input is the slip velocity of each wheel Δv_{ij}. The mono-physical coupling element stacked orange squares pictogram in Fig. 2 is described by (10) in which the power balance is confirmed by the existence of the item dissipated power $\Delta v_{ij} F_{d,ij}$ [9].

7) Chassis: After the forces applied in each wheel $F_{d,ij}$ are determined, the total traction force $F_{d,tot}$ applied to the vehicle at the chassis coupling can be calculated by (11). This is represented as a mono-physical coupling element in Fig. 2.

Applying the second Newton's law to the vehicle chassis dynamic equation, v_{ev} is computed based on the total traction force and the resistant force given by (12). The vehicle chassis dynamic block is described as a accumulation element stacked orange squares pictogram in EMR.

8) Environment: Rolling resistance force, air drag resistance force, and gravity resistance force generated by slope make up the total resistance force imposed by the environment on the vehicle given by (13), with k_{roll} the rolling resistance coefficient, g the acceleration due to gravity, α the slope rate, ρ air density, c_d the air drags coefficient, v_{wind} the wind velocity and A_x the equivalent frontal area of the vehicle. The environment is represented as a source element green oval pictogram in Fig. 2.

With the mathematical equations in Table I and Table II, the EMR of the studied EV and the two motors is built starting from the battery pack to the environmental forces using the EMR rules [10]. Fig 2 presents the complete EMR of the studied EV.

III. Estimation and Control EV

A. Estimation

The gearbox torque and speed $(\hat{T}_i, \hat{\omega}_i)$, and the wheel torque and speed $(\hat{T}_{ij}, \hat{\omega}_{ij})$ is estimated from (4) and (5).

Next, the observers are employed to obtain driving forces for the feedback loops. In this study, the basic disturbance observer (22) in Table III is directly inverted from the equivalent dynamic equation for each wheel, in which a low-pass filter (LPF) is used to suppress the high harmonics of the sensors.

The stator current in d-q frame of the EMs is estimated through the measurement of the AC current of the motor and coordinate transformation (23). The values of the EMF $\hat{\boldsymbol{e}}_{dq,i}$, the rotor flux of IM $\hat{\lambda}_{rd,1}$, the rotor position $\hat{\theta}_i$, and the motor torque $T_{m,i}$ can also be estimated from (18), (19), (20), and (21), respectively.

B. Control Organization

To develop the control scheme for the studied EV, the tuning path $(T_{m,i} \Rightarrow T_i \Rightarrow T_{ij} \Rightarrow \omega_{ij} \Rightarrow F_{d,ij} \Rightarrow F_{d,tot} \Rightarrow v_{ev})$ is defined following the EMR formalism (Fig. 2). The controlled variable is v_{ev}. Based on the causality principle, the force applied to each wheel $F_{d,ij}$ should be controlled during traction. Therefore, the tuning variables are the reference torques for each powertrain $T_{m,i}^*$.

The control scheme can be systematically performed by the inversion-based control of the powertrain with the starting point being the controlled variable [6]. From there, the control scheme is defined by backwards inverting of each block found in the tuning path until each tuning variable has appeared on the control path $(v_{ev}^* \rightarrow F_{d,tot}^* \rightarrow F_{d,ij}^* \rightarrow \omega_{ij}^* \rightarrow T_{ij}^* \rightarrow T_i^* \rightarrow T_{m,i}^*)$. The equations given in this subsection are the results of the above modelling, and they are used to create the control organization of the system in Table III.

In the control of vehicle dynamics, (12) is the first element to be inverted to obtain the velocity control loop. Since an accumulation element cannot be directly reversed, (12) is

TABLE. III
EQUATIONS FOR CONTROL OF THE STUDIED SYSTEM

Estimation

$$\hat{F}_{d,ij} = \left(\hat{T}_{ij} - \mathrm{s}\widetilde{J}_{\omega,ij}\hat{\omega}_{ij}\right)\frac{1}{R_{wh,ij}} \cdot \frac{1}{\tau \mathrm{s}+1} \quad (22)$$

$$\hat{\boldsymbol{i}}_{dq,i} = \begin{bmatrix} \hat{i}_{sd,i} \\ \hat{i}_{sq,i} \end{bmatrix} = \boldsymbol{T}_{PC} \begin{bmatrix} 1 & 0 \\ 0 & 1 \\ -1 & -1 \end{bmatrix} \boldsymbol{i}_{em,i_{meas}} \quad (23)$$

Control Organization

$$F^*_{d,tot} = \hat{F}_{res} + k_{I,v}\int_0^t \left(v^*_{ev} - v_{ev}\right)\mathrm{d}t - k_{P,v}\left(v^*_{ev} - v_{ev}\right) \quad (24)$$

$$F^*_{d,ij} = k_{d,ij}F^*_{d,tot}, \text{ with} \sum_{i=1}^{2}\sum_{j=1}^{2} k_{d,ij} = 1 \quad (25)$$

$$\omega^*_{ij} = \frac{R_{wh,ij}}{\widetilde{J}_{\omega,ij}}\int_0^t \left(F^*_{d,ij} - \hat{F}_{d,ij}\right)\mathrm{d}t \quad (26)$$

$$T^*_{ij} = R_{wh,ij}\hat{F}_{d,ij} + k_{I,\omega}\int_0^t \left(\omega^*_{ij} - \omega_{ij}\right)\mathrm{d}t + k_{P,\omega}\left(\omega^*_{ij} - \omega_{ij}\right) \quad (27)$$

$$T^*_i = k^{-1}_{dif,ij}T^*_{ij} \quad (28) \qquad T^*_{m,i} = k^{-1}_{gb,i}T^*_i \quad (29)$$

TABLE. IV
PARAMETERS OF ECOMMANDER PLATFORM

Parameter [Unit]	Value
Equivalent vehicle mass m [kg]	857
Height of the center of gravity h_{CG} [m]	0.85
Distance of front axle from CG l_f [m]	0.865
Distance of rear axle from CG l_r [m]	1.058
Front wheels track width of the vehicle d_f [m]	1.257
Rear wheels track width of the vehicle d_r [m]	1.219
Effective radius of tire $R_{w,i}$ [m]	0.318
Equivalent inertia moment of the wheel $\widetilde{J}_{\omega,i}$ [kg × m^2]	0.55
Drag coefficient c_d	0.65
Equivalent frontal area A_x [m^2]	2

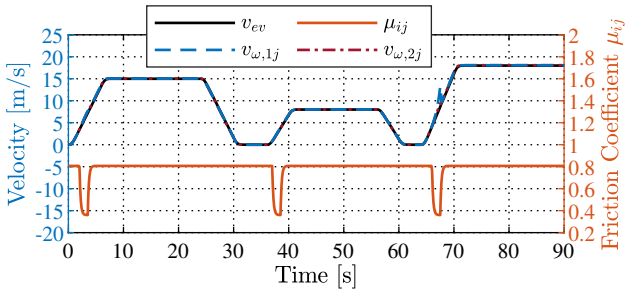

Figure. 4. Longitudinal speeds of the body vehicle and the wheels.

indirectly inverted into an proportional-integral (PI) velocity controller that is given by (24), where $F^*_{d,tot}$ is the reference of the total force applied to the vehicle, $k_{I,v}$ and $k_{P,v}$ are the PI coefficients, $\hat{F}_{res}$ is the resistant force of the environment which is assumed to be measurable or estimable using (13), and v^*_{ev} is the reference velocity. This is a closed-loop control with the measurement of the vehicle velocity v_{ev} as the feedback signal. The PI velocity controller is represented by an indirect inversion in EMR.

Then, $F^*_{d,tot}$ is distributed into the reference traction forces of each wheel as (25). In which $k_{d,ij}$ are the distribution ratios which depends on vehicle operating conditions. This is described by a coupling inversion in EMR.

Due to the use of "magic formula", its model cannot be directly inverted, indirect inversion is demanded. The reference angular speed ω^*_{ij} is defined by the equivalent dynamic equation for each wheel (26) that is illustrated by indirect inversion in EMR, with the estimated traction force $\hat{F}_{d,ij}$ as the feedback signal. The reference angular speed ω^*_{ij} is expressed by (26). The indirect inversion of (6) is performed by a conventional proportional-integral (PI) angular speed controller, which is shown as (27), where $k_{P,\omega}$ and $k_{I,\omega}$ are the PI coefficients. This is a closed-loop control with the estimation of the wheel angular speed $\hat{\omega}_{ij}$ from the angular speed of motor $\omega_{m,i}$ as the feedback signal. The traction force of each wheel $\hat{F}_{d,ij}$ is estimated by (22) and is used as a feedforward signal. This is symbolised by an indirect inversion in EMR. Then, the reference torque T^*_{ij} of each wheel is used to calculate the reference torque of each gearbox T^*_i (28) and the reference torque of each motor $T^*_{m,i}$ (29).

The bottom part of Fig. 2 shows the maximal control organization for the studied vehicle. Similar to control organization for the studied vehicle, the control structure for traction motors in Fig. 3 was designed using an the inversion-based control principle. Here, the reference d-axis current $i^*_{sd,i}$ is obtained by the optimal flux-weakening strategy with IM [11] or by the maximum torque-per-amp (MTPA) strategy with PMSM [12].

IV. EVALUATION TEST AND DISCUSSION

A. Simulation Setting

In this section, the simulation is carried out in the MATLAB/Simulink® environment to evaluate the performance of developed model of AWD-EVs. The parameters of the studied vehicle are listed in Table IV, and its modeling is depicted in Fig. 2. The reference speed of EV is a part of the new European driving cycle (NEDC) test. The longitudinal speed v_{ev} is shown in Fig. 4. The speed v_{ev} is divided into four stages: acceleration (2.5 m/s^2 in 0 $\sim$ 6s, 2 m/s^2 in 36 $\sim$ 40s, 3 m/s^2 in 64 $\sim$ 70s), constant speed, deceleration and zero speed. In the case of this study, the tire friction coefficient was low in the middle of the acceleration stages. As shown in Fig. 4, the road friction coefficient reduces from the high value of 0.807 to the low value of 0.360 for three times.

B. Results and Discussion

Fig. 4 depicts not only the velocity response of the studied EV v_{ev} but also the speed of the wheels $v_{\omega,ij} = R_{wh,ij}\omega_{ij}$. In which $v_{\omega,1j}$ is the speed of the front wheels and $v_{\omega,2j}$ is the speed of the rear wheels. When the friction coefficient of the road surface μ_{ij} decreases, this causes the frictional force to fall. As a result, the vehicle velocity v_{ev} will reduce so it is smaller than the reference velocity v^*_{ev}. As depicted in the control structure in Fig. 2, the velocity controller will rise $F^*_{d,tot}$, which produces the required torque of each motor

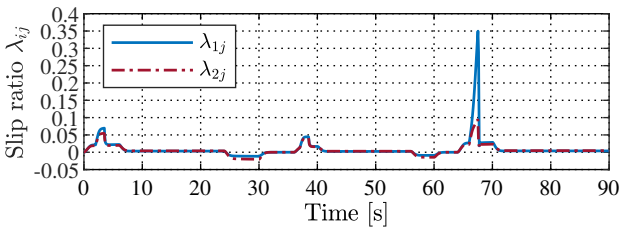

Figure. 5. Slip ratio of the wheels.

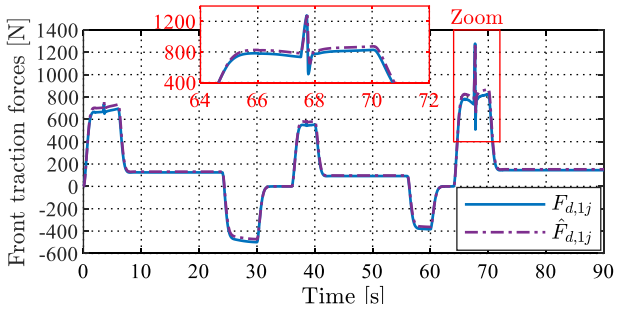

Figure. 6. The wheel traction forces of the front axle.

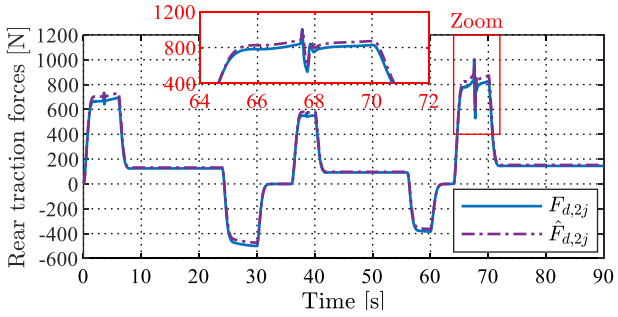

Figure. 7. The wheel traction forces of the rear axle.

also increased. Therefore, the wheel speeds $v_{\omega,ij}$ will increase dramatically on the low-friction coefficient of the road shown in Fig. 4. The vehicle will lose stability if the low-friction track is long and the EV is not equipped with an anti-slip system.

The different stages in the case of this study are evident in the slip ratio of the wheels in Fig. 5, in which λ_{1j} is the slip ratio of the front wheels and λ_{2j} is the slip ratio of the rear wheels. In the road with good friction coefficient ($\mu_{ij} = 0.807$) and stable vehicle speed, the slip ratio of the wheels is always less than 0.004. When the studied vehicle is accelerating or decelerating on a good friction road, the magnitude of the slip ratio is raised but always less than $|0.03|$. However, the slip ratio of the wheels will increase suddenly if the vehicle is accelerated on a slippery road surface. As in the case of this study, the slip ratio of the two front wheels increased to 0.35 when the vehicle had an acceleration of 3 $\mathrm{m/s^2}$ at 66 s in the low-friction track. On the other hand, when the friction coefficient was lowered at the time 2 s and 37 s, the slip ratio only grew to 0.07 in this study. This is because the studied vehicle acceleration in these two times is only 2.5 $\mathrm{m/s^2}$ and 2 $\mathrm{m/s^2}$ at 2 s and 37 s, respectively.

The traction forces and its estimated value of each wheel on the front axle are shown in Fig. 6. Meanwhile, Fig. 7 describes the same variables on the rear axle. At a constant vehicle velocity, each wheel only needs to maintain a small traction force, which is less than 150 N in this study. However, the traction forces of each wheel need to increase when the EV accelerates. The larger the desired acceleration value, the larger the traction forces. For example, when the studied vehicle needs an acceleration of 3 $\mathrm{m/s^2}$ at 65 s, the traction force of each wheel should be about 800 N.

V. Conclusion and Future Works

This paper presents modelling of an AWD-EV controlled in longitudinal motion. Besides the description of the dynamic components and the tire-road interaction of the studied vehicle, the paper also provides in detail the dynamic model of the dual-motor including IM and PMSM. The EMR is used to represent the system, so that control design and strategy development are intuitive and systematic. The model is used in simulation on MATLAB/Simulink® on the road with a variable coefficient of friction. In the future, the model will be validated by comparing with the data obtained from a commercial software and experiments. Then, it can be used to develop different motion control techniques.

References

[1] B.-M. Nguyen, H. Van Nguyen, M. C. Ta, and M. Kawanishi, "Longitudinal Modelling and Control of In-Wheel-Motor Electric Vehicles as Multi-Agent Systems," Energies, vol. 13, no. 20, p. 5437, Oct. 2020.

[2] M. C. Ta, A.-T. Nguyen, B.-M. Nguyen, P. Messier, and J. P. F. Trovao, "Four-wheel Independently Driven Formula: Experimental EV for Motion Control Studies," in 2022 IEEE Energy Conversion Congress and Exposition (ECCE), Oct. 2022

[3] C. Xu, X. Guo, and Q. Xun, "Loss Minimization Based Energy Management for a Dual Motor Electric Vehicle," in 2022 IEEE Transportation Electrification Conference and Expo, Asia-Pacific (ITEC Asia-Pacific), Oct. 2022.

[4] K. Cao et al., "All-Wheel-Drive Torque Distribution Strategy for Electric Vehicle Optimal Efficiency Considering Tire Slip," IEEE Access, vol. 9, pp. 25245-25257, 2021.

[5] H.-W. Kim et al., "A Novel Torque Matching Strategy for Dual Motor-Based All-Wheel-Driving Electric Vehicles," Energies, vol. 15, no. 8, p. 2717, Apr. 2022.

[6] A. Bouscayrol *et al.*, "Multi-converter multi-machine systems: application for electromechanical drives," Eur. Phys. J. - Appl. Phys., vol. 10, no. 2, pp. 131–147, 2000.

[7] K. H. Nam, AC Motor Control and Electrical Vehicle Applications, 2nd ed., CRC Press, 2018.

[8] H. B. Pacejka, Tire and Vehicle Dynamics, 3rd ed., Elsevier, 2006.

[9] B-H. Nguyen, D. Nguyen, V. D. Thanh, and M. C. Ta, "An EMR of Tire-Road Interaction Based-On Magic Formula for Modeling of Electric Vehicles," 2015 IEEE Vehicle Power and Propulsion Conference, 2015.

[10] A. Bouscayrol, J. P. Hautier, and B. Lemaire-Semail, "Graphic formalisms for the control of multi-physical energetic systems: COG and EMR," in *Systemic Design Methodologies for Electrical Energy Systems: Analysis, Synthesis and Management*, X. Roboam, Ed. London, U.K.: ISTE Ltd., 2013, pp. 89–124.

[11] C. T. P. Nguyen, B-H. Nguyen, J. P. F. Trovão, and M. C. Ta, "Effect of battery voltage variation on electric vehicle performance driven by induction machine with optimal flux-weakening strategy," IET Electr. Syst. Transp., vol. 10, no. 4, pp. 351-359, Dec. 2020.

[12] M. C. Ta and A.-T. Nguyen, "Advanced control algorithms for electric machine drives," in *Encyclopedia of Electrical and Electronic Power Engineering*, Elsevier, pp. 454-471, 2023.